

---

# Autoradiographic Method for Quantitation of Radiolabeled Proteins in Tissues Using Indium-111

Eric M. Morrel, Ronald G. Tompkins, Alan J. Fischman, Robert A. Wilkinson, John F. Burke, Robert H. Rubin, H. William Strauss, and Martin L. Yarmush

*The Surgical Service of the Massachusetts General Hospital, Department of Surgery, and The Nuclear Medicine Division of the Massachusetts General Hospital, Department of Radiology, Harvard Medical School, Boston, Massachusetts*

A quantitative autoradiographic method was developed to measure  $^{111}\text{In}$ -labeled proteins in extravascular tissues with a spatial resolution sufficient to associate these proteins with tissue morphology. A linear relationship between measured grain density and isotope concentration was demonstrated with uniformly-labeled standard sources of epoxy-embedded gelatin containing [ $^{111}\text{In}$ ]albumin; half-distance of spatial resolution was  $0.6\ \mu\text{m}$ . The technique was illustrated by measuring 24-hr accumulation of diethylenetriaminepentaacetic acid-coupled  $^{111}\text{In}$ -labeled human polyclonal IgG and human serum albumin (HSA) in a thigh infection model in the rat. Gamma camera images localized the infection and showed target-to-background ratios of  $2.5 \pm 0.3$  for IgG and  $1.4 \pm 0.02$  for human serum albumin (mean  $\pm$  s.d.,  $n = 3$ ). Using quantitative autoradiography, significantly higher average tissue concentrations were found in the infected thighs at 4 to 4.5% of the initial plasma concentrations as compared to 0.2 to 0.3% of initial plasma concentrations in the noninfected thigh ( $p < 0.05$ ); these radiolabeled proteins were not inflammatory cell associated and localized primarily within the edematous interstitial spaces of the infection.

J Nucl Med 30:1538-1545, 1989

---

Over the past several years, radiolabeled antibodies have been used clinically for the external imaging of tumors, myocardial necrosis, pulmonary emboli, and infection (1-12). Currently, the methods for screening potential antibodies for immunoscintigraphic applications include: in vitro cell binding, biodistribution studies, and external imaging in small animals. In order to optimize the screening process, a better understanding of the in vivo localization of radiolabeled antibodies within tissues at the light microscopic level is critical.

While immunoscintigraphy with conventional single photon agents is useful for localizing focal sites of pathology, absolute tissue concentration of radiolabeled protein cannot be determined. In addition, external imaging does not provide any information about the distribution of radioactivity in different tissue spaces or cell types. For example, in myocardial infarction im-

aging, it is impossible to determine the distribution of anti-myosin between necrotic myocytes, normal myocytes, inflammatory cells, and interstitial space.

Recently, a method of quantitative autoradiography was developed to measure concentrations of radioiodinated proteins in microscopic volumes of tissue and to determine the degree of association of radiolabel with different microscopic tissue components (13). This method was recently used to determine iodine-125- ( $^{125}\text{I}$ ) labeled low-density lipoprotein (LDL) tissue concentrations in vascular (14) and extravascular tissues (15).

Since indium-111 ( $^{111}\text{In}$ ) is the most commonly used radionuclide in immunoscintigraphy, this autoradiographic method was adapted to  $^{111}\text{In}$ -labeled proteins. The method was used to measure tissue concentrations of these  $^{111}\text{In}$ -labeled proteins in an effort to better understand mechanisms that localize radiolabeled proteins in immunoscintigrams. Indium-111 decays by electron capture and thus does not have direct particulate emission, however, significant quantities of very low energy internal conversion and Auger electrons are

---

Received Jan. 27, 1989; revision accepted June 7, 1989.

For reprints contact: Ronald G. Tompkins, MD, ScD, ACC 3A Suite 364, Massachusetts General Hospital, Boston, MA 02114.

produced during decay. The low energy of these emissions make it possible to obtain autoradiograms of sufficient resolution to localize radioactivity to specific cell types and to provide quantitation of local protein concentrations.

The present report illustrates the method by using  $^{111}\text{In}$ -labeled polyclonal human IgG as a model antibody to evaluate the potential of  $^{111}\text{In}$  quantitative autoradiography. This antibody preparation has been demonstrated to be an effective agent for external imaging of focal sites of infection in both animal models of infection and in human subjects by a mechanism that is not known (17). Possible mechanisms for localization include an enhanced specific binding of antibody to tissue components such as Fc receptors on the surface of leukocytes or simply increased vascular permeability that naturally occurs in infected tissues. By quantitatively comparing the localization of  $^{111}\text{In}$ -IgG with that of  $^{111}\text{In}$ -labeled human serum albumin (a vascular permeability marker) at focal sites of infection, these two possibilities may be distinguished.

## METHODS

### Antibodies

Human nonspecific polyclonal IgG (Sandoz, Inc., East Hanover, NJ) containing IgG antibodies that normally occur in a broadly-based donor population was used. This preparation (Sandoglobulin) is 96% IgG with a distribution of subclasses corresponding to normal serum.

Sandoglobulin and human serum albumin (HSA) (Cutter Biologicals, Berkeley, CA) were radiolabeled with  $^{111}\text{In}$  via the diethylenetriamine pentaacetic acid (DTPA) antibody chelate method (16). Briefly, isobutylchloroformate (0.25 mmol) were added to a cooled solution of the triethylamine salt of DTPA (0.2 mmol in 2 ml of acetonitrile) and stirred for 30 min. An aliquot of the resulting solution of the mixed carboxy anhydride of DTPA was added to a cooled solution of antibody dissolved in 0.1 M  $\text{NaHCO}_3$ , pH 7 to 8. After overnight storage at 4°C, the mixture was dialyzed against 0.1M acetate buffer pH 5.0 and applied to a Sephadex G-25 column. The protein fractions were dialyzed against normal saline. A 0.5-ml aliquot of the resulting antibody solution, containing ~0.5 mg of protein, was diluted with 0.5 ml 1.0M citrate buffer (pH 5.0), combined with 1–2 mCi of indium chloride (Amersham, Arlington Heights, IL), incubated for 30 min at room temperature, and applied to a Sephadex G-25 column to isolate protein fractions.

### Animal Model

A clinical isolate of *E. Coli* was stored at -70°C in a freezing media containing 20% glycerol and 80% dextrose phosphate until use. Aliquots of bacteria were defrosted and colony counts performed on serial dilutions grown overnight on BBL Brucella agar plates. Based on the colony count, freshly thawed bacterial suspensions were washed and diluted with saline to a final concentration of  $8 \times 10^{10}$  organisms/ml. Aliquots (0.1 ml) of bacterial suspensions ( $8 \times 10^9$  organisms) were injected into the right thigh muscle of 150 g male Sprague-Dawley rats

(Charles River Breeding Laboratories, Burlington, MD). Twenty-four hours later, gross swelling in the right thigh readily appeared representing ~5% of the total-body weight of the animal. Twenty-four hours after bacterial inoculations, 500  $\mu\text{g}$  of antibody or human serum albumin (specific activity ~3  $\mu\text{Ci}/\mu\text{g}$  for either tracer) was injected via the tail vein. Tail vein blood samples were collected at 10 min, 4 hr, 20 hr, and prior to killing at 25 hr. At 24 hr after injection of the radionuclide, the animals were anesthetized with ketamine and scintigrams recorded using a standard field-of-view scintillation camera (Technicare 420, Solon, OH) equipped with a parallel hole, medium energy collimator. Images were recorded for a preset time of 2 min per view. Following imaging, the animals were killed and pressure-perfusion fixed for 20 min with 2.5% glutaraldehyde in 0.1M sodium cacodylate, pH 7.4. Portions of the infected and noninfected thigh muscle were excised and stored overnight in fresh fixative. The following day, whole tissue  $^{111}\text{In}$  counts of the excised thigh muscle samples and total plasma radioactivities ( $C_p$ , cpm/ml) were measured in a gamma counter (Compugamma, LKB Pharmacia; counting efficiency, 80%).

### Autoradiography

The autoradiography protocol has been presented in detail elsewhere (13, 14). Briefly, glutaraldehyde-fixed samples were cut into small cubes (~3 mm on edge), processed by routine histological techniques of postfixation with osmium tetroxide, dehydration in graded alcohols, and embedded in epoxy resin (EMbed 812, Electron Microscopy Sciences, Ft. Washington, PA). These plastic-embedded samples were trimmed to a small trapezoid, (~0.5 mm on a side), 1- $\mu\text{m}$  sections were cut with glass knives on an ultramicrotome (Sorvall MT-2, DuPont, Newton, CT) and 10 to 15 sections were placed in a central location on a microscope slide.

Within 3 days of the in vivo experiment (approximately one half-life of  $^{111}\text{In}$ , 2.83 days), the slides were dipped in molten (40°C) nuclear emulsion (Kodak NTB-2; Eastman Kodak, Rochester, NY) in a darkroom and dried vertically at 27–28° and 80% relative humidity for 1 hr. After packaging in light-tight boxes containing desiccant (anhydrous calcium sulfate), the slides were stored for 14–21 days at 4°C. Slides were developed, stained with 0.5% toluidine blue, and allowed to dry.

Grain density measurements were made visually using a Zeiss Photomicroscope III (Carl Zeiss, New York, NY) and a calibrated eyepiece reticle grid containing rectangular boxes ( $5.6 \times 28 \mu\text{m}$  at 880X). Transmitted light brightfield or darkfield microscopy was used for grain density measurements. At least ten tissue sections from each embedded tissue sample were counted and at least two tissue samples from each thigh were quantitatively analyzed.

Nonradioactive tissue sections of similar structure to that being analyzed were included with each group on a separate slide as a control for positive or negative chemography. Chemography is the subsequent development of autoradiographic grains as a result of chemical reduction of the silver halide within the nuclear emulsion rather than as a result of a radioactive decay event. Such artifactual grains can greatly increase background grain densities and thereby reduce detection sensitivity of radioactive decay.

To provide a relationship between measured grain density and  $^{111}\text{In}$  concentration, uniformly-labeled standards were

prepared as previously reported (13) using [ $^{111}\text{In}$ ]HSA. Briefly, 1-ml aliquots of known concentrations of [ $^{111}\text{In}$ ]HSA in 0.15M NaCl were added to identical volumes of 14% (w/v) gelatin in water at 37°C. The mixtures were transferred to individual plastic vials and allowed to gel at 4°C for 8 hr after which 10 ml of 2.5% (w/v) glutaraldehyde in 0.1M cacodylate buffer was added to each vial and stored at 4°C overnight. The fixed gels were removed from the vials, cut into small cubes (~3 mm on edge), and processed for embedding as outlined above for the tissue samples. Samples at each concentration were cut out of the epoxy resin blocks, weighed, and analyzed for radioactivity in a gamma counter (CompuGamma) creating a series of gelatin standards.

These standard calibration samples were dipped, exposed, and developed at the same time with each group of slides containing radioactive tissues. The calibration data was used to convert the measured silver grain density over 1  $\mu\text{m}$  tissue sections into absolute tissue isotope concentration  $C_T$  (cpm/ml). Calculated tissue concentrations were normalized to the 10-min plasma concentration at the time of the experiment,  $C_{Po}$  (cpm/ml), to yield the relative tissue concentration  $C_T/C_{Po}$ .

As previously described for  $^{125}\text{I}$  (13), resolution of  $^{111}\text{In}$  autoradiography was assessed using high concentration  $^{111}\text{In}$  gelatin standards to produce a step change from a uniformly labeled high concentration standard to an immediately adjacent nonradiolabeled plastic epoxy resin thus, creating a resolution target. Sections, consisting of roughly half embedded radioactive gelatin and half pure nonradioactive epoxy resin, were autoradiographed. The calibrated eyepiece reticle (used at a magnification of 220X corresponding to grid boxes  $2.2 \times 11 \mu\text{m}$ ) was used to measure the grain density over the gelatin as a function of distance. From these measurements, a half-distance (distance from the edge of the  $^{111}\text{In}$ -labeled source at which the grain density falls to half of its value over the source) was obtained.

Statistical comparison of populations was performed by Student's unpaired t-tests (two-way). A probability of a type 1 error of 5% or less was considered significant.

## RESULTS

The resolution of  $^{111}\text{In}$  autoradiography was determined by measurement of grain densities from the edge of a uniformly-labeled  $^{111}\text{In}$  gel to background grain density levels. An autoradiogram of a uniformly labeled  $^{111}\text{In}$  gel along with a plot of the normalized grain densities is shown in Figure 1. Grain densities decreased to half the average level over the uniformly-labeled gelatin source yielding a half-distance of 0.6  $\mu\text{m}$ . The average grain density over the  $^{111}\text{In}$ -labeled gel was 6.6 grains/ $24.2 \mu\text{m}^2$  and over the nonradioactive adjacent epoxy (representing background grain density) was 0.75 grains/ $24.2 \mu\text{m}^2$ . A standard curve, relating autoradiographic grain density (grains/ $1000 \mu\text{m}^2$ ) to  $^{111}\text{In}$  concentrations (cpm/ml), is shown in Figure 2. As is readily apparent, the data was described satisfactorily by a linear model with an  $R^2$  of 0.99.

Plasma clearance of  $^{111}\text{In}$ -labeled HSA was more

rapid than [ $^{111}\text{In}$ ]IgG (Fig. 3). After 25 hr of tracer circulation, plasma  $^{111}\text{In}$ -IgG and [ $^{111}\text{In}$ ]HSA associated radioactivity averaged 26% and 13% of initial levels. [ $^{111}\text{In}$ ]HSA plasma concentration were also less than those of [ $^{111}\text{In}$ ]IgG at 2 and 20 hr.

Representative gamma camera images after injection of either [ $^{111}\text{In}$ ]IgG or [ $^{111}\text{In}$ ]HSA are shown in Figure 4. These images demonstrate that both radiolabeled proteins preferentially localize to the infected thighs. Corresponding average counts per pixel were  $582 \pm 58$  in the infected thigh versus  $233 \pm 10$  in the noninfected thigh for [ $^{111}\text{In}$ ]IgG, and  $519 \pm 68$  in the infected thigh versus  $371 \pm 31$  in the noninfected thigh for the [ $^{111}\text{In}$ ]HSA (Mean  $\pm$  s.d.,  $n = 3$ ). A significant difference ( $p < 0.05$ ) between the counts per pixel in the infected and noninfected thighs for both [ $^{111}\text{In}$ ]IgG and [ $^{111}\text{In}$ ]HSA was demonstrated. The target-to-back-

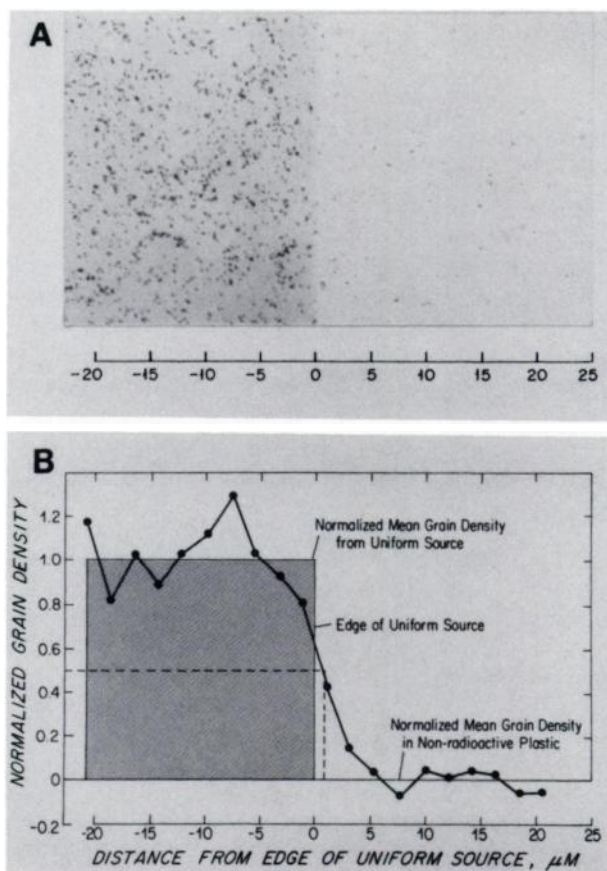


**FIGURE 1**

Half-distance measurement of the  $^{111}\text{In}$  autoradiography method. A: Autoradiogram of epoxy-embedded uniformly-labeled source consisting of [ $^{111}\text{In}$ ]HSA in gelatin on the left half and nonradioactive epoxy on right. B: Grain densities, measured by visual grain counting at 2200X, over the uniformly-labeled source and immediately adjacent epoxy (Mean  $\pm$  s.d.,  $n = 4$ ). Densities normalized with respect to the mean grain density over the  $^{111}\text{In}$ -labeled source. Half-distance at which the grain density falls to 50% of the mean grain density over the source (0.6  $\mu\text{m}$ ) indicated by the dashed lines.

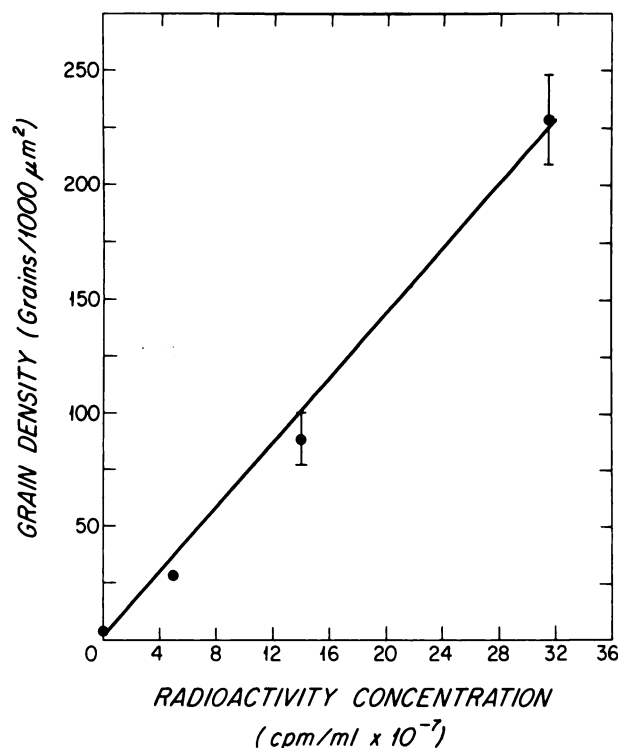


**FIGURE 2**

Representative standard calibration curve. Visually counted grain densities over a series of epoxy-embedded uniformly-labeled gelatin standards plotted versus radioactivity concentration in the embedded standard sources of a [<sup>111</sup>In]IgG or [<sup>111</sup>In]HSA experiment; at least 1000 grain/gel concentration were counted. (Mean ± s.d.)

ground ratio (ratio of the counts per pixel in the infected and noninfected thighs) was determined for each animal. The average target to background ratio for [<sup>111</sup>In]IgG was  $2.5 \pm 0.3$  and for [<sup>111</sup>In]HSA as  $1.4 \pm 0.2$  (Mean ± s.d.,  $n = 3$ ). These ratios were significantly greater than unity ( $p < 0.05$ ) indicating preferential localization of radiolabel at the infection sites.

Representative autoradiograms of tissue samples from infected and uninfected thighs are shown in Figure 5. The noninfected muscle tissue, shown in Panels A and B, exhibits normal skeletal muscle morphology; muscle fibers within each fascicle are tightly packed with little space between fibers. No morphological features of infection, such as cellular infiltration by neutrophils and/or edema were visible in the sections from uninfected high muscle. By contrast, infected tissue (Panels C and D) displayed significant cellular infiltration that consisted primarily of neutrophils within loose, edematous interstitial connective tissue.

Qualitatively, the autoradiographic silver grain densities were distinctly different over the infected (Panel B) versus uninfected muscle (Panel D). The distribution of these grains was nearly identical for IgG and albumin. Silver grain densities were low, often at or near background levels, over the noninfected soft tissues. How-

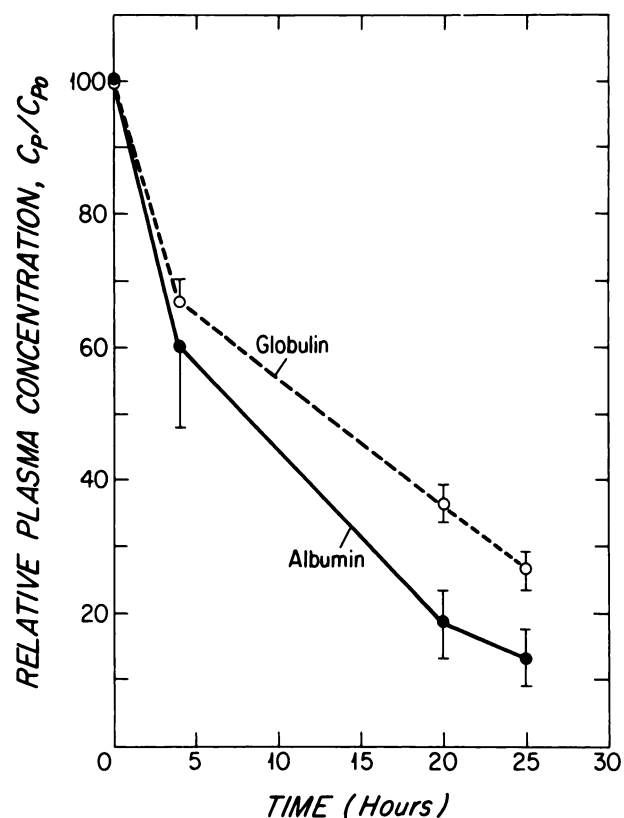


**FIGURE 3**

Plasma decay curves. [<sup>111</sup>In]IgG and [<sup>111</sup>In]HSA (albumin) concentration in plasma ( $C_P$ ) as a function of time. Concentration are expressed as a percentage of the labeled IgG or HSA concentration measured 10 min after tracer injection ( $C_{P0}$ ). (Mean ± s.e.m.,  $n = 3$ )

ever, grain densities in autoradiograms of infected tissue were uniformly greater than background, particularly within the connective tissues surrounding muscle bundles. No particular tendency for an association between grains and any tissue component such as the leukocytes was seen. Grain densities over the muscle bundles varied from background levels to levels that were indistinguishable from the high grain densities of the surrounding interstitial space.

Using the standard curve (Fig. 2), tissue concentrations ( $C_T$ ) were estimated from grain densities measured over the tissues. Tissue concentrations were normalized and expressed as relative tissue concentrations ( $C_T/C_{P0}$ ). Averages of relative tissue concentrations representing six regions for infected and noninfected tissues within an animal (animal averages) were combined for three animals to yield grand animal averages (Fig. 6). The animal average tissue concentrations of both IgG and albumin within infected thighs ranged from 4.0 to 4.5% of  $C_{P0}$ . This represents an actual tissue protein concentration (with a  $C_{P0}$  of  $1.2 \times 10^8$  dpm/ml and a specific activity of  $3 \mu\text{Ci}/\mu\text{g}$ ) of 0.73 to 0.82  $\mu\text{g}/\text{ml}$ . Animal average tissue concentrations in noninfected tissues were significantly less than those in the infected

$^{111}\text{In} - \text{IgG}$

$^{111}\text{In} - \text{HSA}$

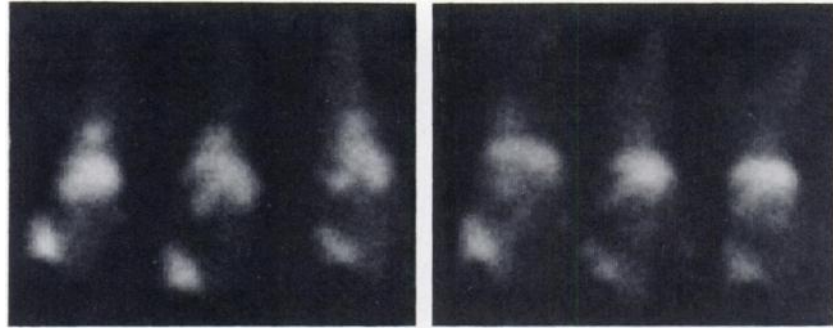


**FIGURE 4**

Scintigrams demonstrating localization of unilateral *E. coli* thigh infections imaged 24 hr after tracer injection of either  $^{111}\text{In}$ -labeled nonspecific polyclonal IgG or HSA.

thighs, averaging 0.2 to 0.3% of the  $C_{\text{PO}}$  ( $p < 0.05$ ). The average target-to-background ratios based upon the individually calculated ratios of infected to noninfected tissue concentration for each animal were  $9.9 \pm 8.7$  for  $^{111}\text{In}$ IgG and  $7.8 \pm 1.1$  for  $^{111}\text{In}$ HSA (Mean  $\pm$  s.d.,  $n = 3$ ).

One major advantage of autoradiography over other methods of tissue concentration measurement is the ability both to localize radiolabel to specific tissue structures and to determine concentrations of radiolabeled proteins that are associated with those tissues. An example of this feature of autoradiography is shown in Figure 7. For both radiolabel tracers, direct quantitative comparisons of the average normalized concentrations measured over the muscle fibers in infected tissues to those concentrations in the region of edematous connective tissue surrounding the fibers may be made. This analysis indicates that concentrations outside of the muscle cells were higher than those over the fibers,

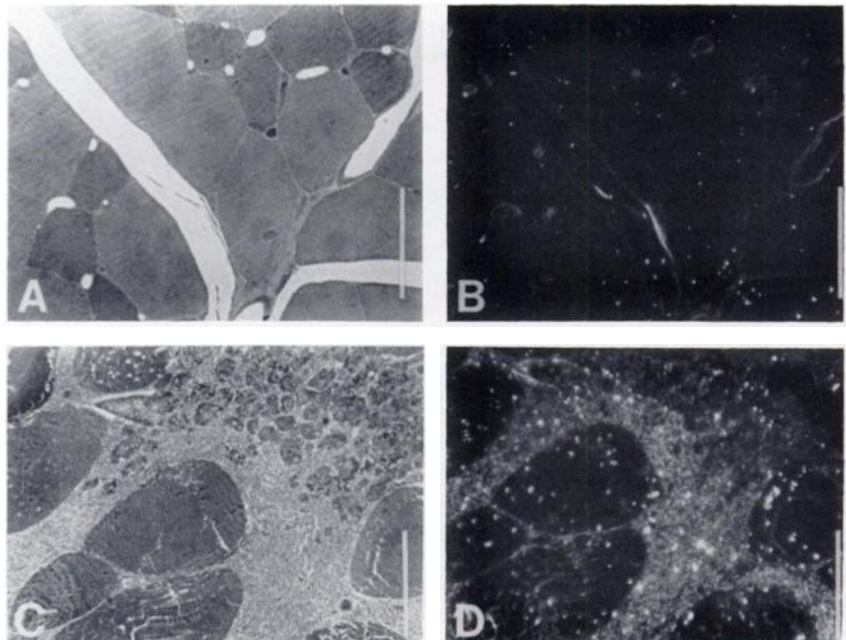
yielding ratios of these concentrations of 1.6 and 1.3 for  $^{111}\text{In}$ IgG and  $^{111}\text{In}$ HSA, respectively.

## DISCUSSION

This study demonstrates the first measurement of  $^{111}\text{In}$ -labeled protein concentrations within microscopic volumes of tissue using quantitative autoradiography and therefore demonstrates a useful method to obtain high tissue resolution of clinically relevant  $^{111}\text{In}$ -labeled proteins. Indium-111 has properties that are particularly well suited for high resolution autoradiography, since its decay is associated with a high yield of very low energy conversion and Auger electrons. Gamma emissions are not effective in producing discrete grains in autoradiographs and do not produce significant background degradation. Indium-111 was used in this study not only because of its potential as a suitable radioactive

**FIGURE 5**

Representative toluidine blue stained autoradiograms of  $^{111}\text{In}$ IgG in non-infected (A, B) and infected (C, D) thigh muscle tissue following 24-hr circulation in the rat. A: Noninfected tissue showing minimal edema and silver grain density. Phase contrast photomicrograph; bar represents 50  $\mu\text{m}$ . B: Darkfield photomicrograph of Panel A. C: Representative infected tissue showing interstitial edema and increased grain density. Phase contrast. D: Darkfield photomicrograph of Panel C showing higher grain densities in the infected tissue; grains primarily localize within the interstitial tissues surrounding muscle fibers.



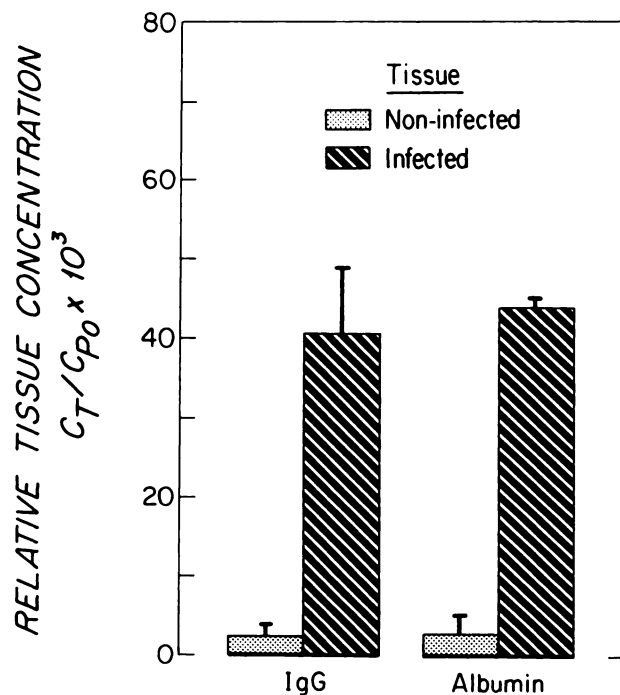


**FIGURE 6**

Grand average relative tissue concentrations ( $C_T/C_{P0}$ ) of  $^{111}\text{In}$ -labeled IgG and HSA within noninfected and infected tissues.  $C_T$  is the concentration within the tissue and  $C_{P0}$  is the radiolabel concentration within the plasma measured at 10 min after tracer injection. (Mean  $\pm$  s.e.m.,  $n = 3$ )  $C_T$  for the radiolabel proteins in infected tissue was greatly increased as compared to the noninfected thigh;  $C_T$  for albumin was only slightly higher than  $C_T$  for IgG in both the infected and noninfected thighs.

source for autoradiography but also because it is currently the most commonly used radionuclide for in vivo antibody imaging. Indium-111 is a popular imaging radionuclide for several reasons including: (a) protein labeling via chelating group derivitized intermediates such as DTPA is a relatively simple and reproducible procedure (16); (b)  $^{111}\text{In}$ -labeling is known to be stable intracellularly (17-19); (c) half-life  $^{111}\text{In}$  (2.83 days) is relatively well matched to the long circulation times of antibodies; and (d) gamma emissions of 171 and 247 keV are readily imaged with conventional gamma cameras equipped with medium-energy collimation.

The validity of quantitative autoradiography with  $^{111}\text{In}$ -labeled proteins is demonstrated by the very satisfactory statistical fit of a linear model to the standard curve relating measured autoradiographic grain density to radioactivity concentration. The resolution of  $^{111}\text{In}$  autoradiography, whose half-distance was  $0.6 \mu\text{m}$ , was better than that of  $^{125}\text{I}$  autoradiography, whose half-distance was  $1.7 \mu\text{m}$  as determined by the same method (13). Indium-111 resolution was comparable to a half-distance of  $0.4 \mu\text{m}$  for hydrogen-3 autoradiography as

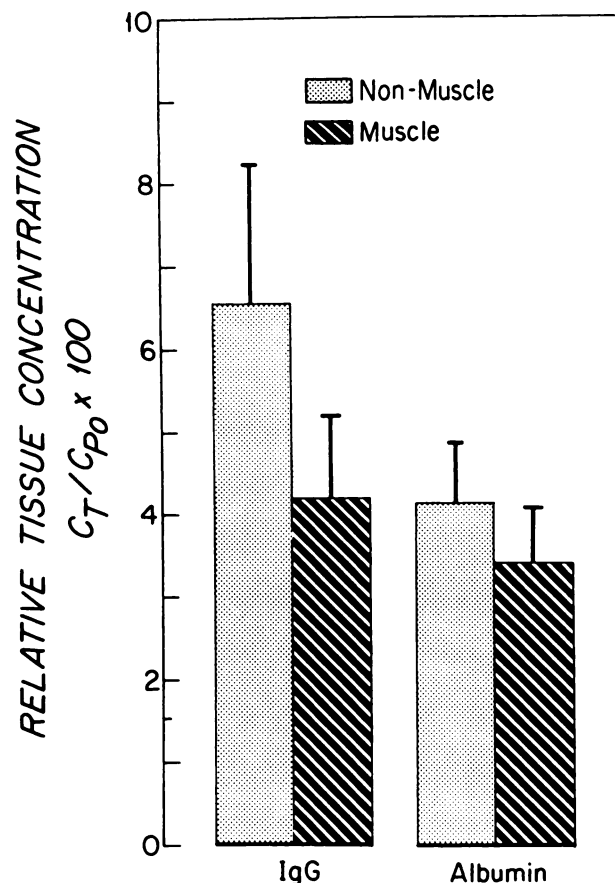


**FIGURE 7**

Average relative tissue concentrations of  $^{111}\text{In}$ -labeled IgG ( $n = 6$ ) and albumin ( $n = 3$ ) within muscular and nonmuscular regions of infected thighs; nonmuscular regions are the interstitial spaces excluding vascular regions; muscular regions are areas occupied by muscles. (Mean  $\pm$  s.e.m.).

reported by Rogers although the exact method for Rogers's half-distance determination is not known (20).

The primary limitation of  $^{111}\text{In}$  autoradiography is the short physical half-life of 2.83 days for  $^{111}\text{In}$ . This rapid decay requires that large amounts of radiolabeled protein are injected and that tissue processing (embedding in plastic and sectioning) is rapid in order to produce autoradiographs with grain densities that are significantly greater than background. In general, this time from the in vivo experiment to placement of the emulsion over the autoradiographic epoxy-embedded tissue sections was approximately one half-life. However, when these conditions are met, accurate tissue concentration measurements and high resolution autoradiograms may be achieved.

The  $^{111}\text{In}$  quantitative autoradiography method was used to further investigate gamma camera studies localizing radiolabeled IgG and HSA to sites of infection in animals and humans (11, 21). Results of gamma camera imaging of focal *E. coli* infections in this study with  $^{111}\text{In}$ -labeled IgG and HSA reproduce those previ-

ously reported observations (11, 21). Both [ $^{111}\text{In}$ ]IgG and [ $^{111}\text{In}$ ]HSA accumulated to an extent sufficient to produce clear images of the infection site, with target-to-background ratios of  $2.5 \pm 0.3$  and  $1.4 \pm 0.02$ , respectively. Quantitative autoradiography of tissue samples from the animals used in these experiments support these imaging results. Tissue radionuclide concentrations, measured relative to initial plasma radioactivity for each animal, were an order of magnitude higher in the infected thigh muscles compared to the noninfected contralateral thighs.

For both IgG and HSA, ratios of radiolabel concentration between the infected and noninfected muscle measured autoradiographically were significantly greater than that measured on the gamma camera images. This difference is most likely the result of inclusion of residual intravascular activity in the imaging-based measurements. Thus, one clear advantage of the autoradiographic method in animal studies is the ability to determine tissue concentrations of radioactivity without the contaminating intravascular radioactivity.

A principal feature of autoradiography is its ability to associate radiolabel concentrations with specific tissue spaces and cell types. In this study, in the infected muscle, accumulation of  $^{111}\text{In}$ -labeled IgG and HSA was observed primarily over the edematous interstitial space in a diffuse pattern that was not inflammatory cell associated. However, in areas with extensive involvement in the infectious process, silver grains were also seen over muscle fibers suggesting that radiolabeled proteins may also have entered some of the muscle spaces possibly as a result of damage to the muscle cell membranes.

One hypothesis to explain the marked accumulations of nonspecific polyclonal IgG within infection is the binding of IgG to Fc receptors on the surface of infiltrating leukocytes (21). As a result of the current study, this hypothesis is not likely for two reasons: (a) if IgG binding to Fc receptors on leukocytes were important, then autoradiographic grains should have been leukocyte-associated; however, the silver grains were not found to be associated with leukocytes and (b) if Fc binding is important for IgG to accumulate within infections then, the total accumulation and tissue distribution of this accumulation for IgG should be very different from albumin which does not have specific Fc binding properties; however, the total accumulation and tissue distribution for albumin and IgG were identical in this study. It has been reported that Fc receptors may be shed from leukocytes within an inflammatory reaction (22), however, the fact that the total accumulation of IgG and albumin were nearly identical strongly argues against any additional specific Fc receptor binding of IgG to shed Fc receptors. Therefore, the Fc receptor binding hypothesis is not only unnecessary to explain IgG accumulation but an unlikely mechanism

for IgG accumulation. An enhanced vascular permeability would lead to accumulation of these macromolecules and would be a more reasonable explanation.

In conclusion, the results of this study establish the feasibility of quantitative autoradiography of tissue samples after injection of  $^{111}\text{In}$ -labeled proteins. This approach can be applied to a variety of problems in which accurate measurements of tissue concentrations of  $^{111}\text{In}$ -labeled radiopharmaceuticals are required. Furthermore, the high resolution of this technique might be of general use in protein autoradiography in instances where the resolution of  $^{125}\text{I}$  autoradiography is not sufficient and tritium labeling is not feasible.

## ACKNOWLEDGMENTS

This work was in part supported by the National Institutes of Health Grant in General Medical Sciences GM 21700 and GM T32-07035, Shriners Hospitals for Crippled Children, the George Link Jr. Foundation, New York, NY, the Edward Mallinkrodt Jr. Foundation, St. Louis, MO, and Ortho-Biotec Imaging Products, Washington's Crossing, NJ.

## REFERENCES

1. Kennan AM. Radiolabeled monoclonal antibodies: current status and future outlook. In: *Nuclear Medicine Annual*. New York: Raven Press, 1988:171-207.
2. Carrasquillo JA, Krohn KA, Beaumier P, et al. Diagnosis and therapy for solid tumors with radiolabeled antibodies and immune fragments. *Cancer Treat Rep* 1984; 68:317-328.
3. Larson SM. Radiolabeled monoclonal anti-tumor antibodies in diagnosis and therapy. *J Nucl Med* 1985; 26:583-545.
4. Larson SM. Lymphoma, melanoma, colon cancer: diagnosis and treatment with radiolabeled monoclonal antibodies. The 1986 Eugene P. Pendergrass New Horizons Lecture. *Radiology* 1987; 165:297-304.
5. Khaw BA, Gold HK, Yasuda T, et al. Scintigraphic quantification of myocardial necrosis in patients after intravenous injection of myosin-specific antibody. *Circulation* 1986; 74:501-508.
6. Khaw BA, Yasuda T, Gold HK, et al. Acute myocardial infarct imaging with indium-111-labeled monoclonal antimyosin Fab. *J Nucl Med* 1987; 28:1671-1678.
7. Rosebrough SF, Grossman ZD, McAfee JG, et al. Thrombus imaging with indium-111 and iodine-131-labeled fibrin-specific monoclonal antibody and its F(ab')<sub>2</sub> and Fab fragments. *J Nucl Med* 1988; 29:1212-1222.
8. Knight LC, Maurer AH, Ammar IA, Shealy DJ, Mattis JA. Evaluation of indium-111-labeled anti-fibrin antibody for imaging vascular thrombi. *J Nucl Med* 1988; 29:494-502.
9. Oster ZH, Srivastava SC, Som P, et al. Thrombus radioimmunoscintigraphy: an approach using monoclonal antiplatelet antibody. *Proc Natl Acad Sci USA* 1985; 82:3465-3468.
10. Locher JT, Seybold K, Andres RY, Schubiger PA,

- Mach JP, Buchegger F. Imaging of inflammatory and infectious lesions after injection of radioiodinated monoclonal anti-granulocyte antibodies. *Nucl Med Commun* 1986; 7:659-670.
11. Fischman AJ, Rubin RH, Khaw BA, et al. Detection of acute inflammation with <sup>111</sup>In-labeled nonspecific polyclonal IgG. *Semin Nucl Med* 1988; 18:335-344.
  12. Fairweather DS, Bradwell AR, Dykes PW, Vaughan AT, Watson-James SF, Chandler S. Improved tumour localization using indium-111 labeled antibodies. *Br Med J* 1983; 287:167-170.
  13. Schnitzer JJ, Morrel EM, Colton CK, Smith KA, Stemerman MB. Absolute quantitative autoradiography of low concentrations of <sup>125</sup>I-labeled proteins in arterial tissue. *J Histochem Cytochem* 1987; 35:1439-1450.
  14. Tompkins RG, Schnitzer JJ, Yarmush ML. Macromolecular transport within heart valves. *Circ Res* 1989; 64:1213-1223.
  15. Tompkins RG, Schnitzer JJ, Yarmush ML, Colton CK, Smith KA. Measurement of <sup>125</sup>I-low density lipoprotein uptake in selected tissues of the squirrel monkey by quantitative autoradiography. *Am J Pathol* 1988; 132:526-542.
  16. Krejcarek GE, Tucker KL. Covalent attachment of chelating groups to macromolecules. *Biochem Biophys Res Commun* 1977; 77:581-585.
  17. Thakur ML, Segal AW, Louis L, Welch MJ, Hopkins J, Peters TJ. Indium-111-labeled cellular blood components: mechanisms of labeling and intracellular location in human neutrophils. *J Nucl Med* 1977; 18:1022-1026.
  18. Meares CF, Goodwin DA, Leung CS, et al. Covalent attachment of metal chelates to proteins: The stability *in vivo* and *in vitro* of the conjugate of albumin with a chelate of <sup>111</sup>indium. *Proc Natl Acad Sci USA* 1976; 73:3803-3806.
  19. Goodwin DA, Meares CF, McCall MJ, et al. Chelate conjugates of monoclonal antibodies for imaging lymphoid structures in the mouse. *J Nucl Med* 1985; 26:493-502.
  20. Rogers AW. Techniques of autoradiography, 3rd edition. New York: Elsevier, 1979:74-75.
  21. Rubin RH, Young LS, Hansen WP, et al. Specific and nonspecific imaging of localized Fisher Immunotype 1 *Pseudomonas aeruginosa* infection with radiolabeled monoclonal antibody. *J Nucl Med* 1988; 29:651-656.
  22. Huizinga TW, Van der Schoot CE, Jost C, et al. The PI-linked receptor FcRIII is released on stimulation of neutrophils. *Nature* 1988; 333:667-669.